

A Highly Selective 3D Spiked Ultraflexible Neural (SUN) Interface for Decoding Peripheral Nerve Sensory Information

Jiahui Wang, Xin Yuan Thow, Hao Wang, Sanghoon Lee, Kai Voges, Nitish V. Thakor,* Shih-Cheng Yen,* and Chengkuo Lee*

Artificial sensors on the skin are proposed as a way to capture information that can be used in intracortical microstimulation or peripheral intraneural stimulation to restore sensory feedback to persons with tetraplegia. However, the ability of these artificial sensors to replicate the density and complexity of the natural mechanoreceptors is limited. One relatively unexplored approach is to make use of the signals from surviving tactile and proprioceptive receptors in existing limbs by recording from their transmitting axons within the primary sensory nerves. Here, a novel spiked ultraflexible neural (SUN) interface that is implanted into the peripheral nervous system to capture sensory information from these mechanoreceptors in acute rat experiments is described. The novel 3D design, which integrates spiked structures for intrafascicular nerve recording with an ultraflexible substrate, enables a unique conformal interface to the target nerve. With the high-quality recording (average signal-to-noise-ratio of 1.4) provided by the electrode, tactile from proprioceptive stimuli can be differentiated in terms of the firing rate. In toe pinching experiments, high spatial resolution classification can be achieved with support vector machine classifier. Further work remains to be done to assess the chronic recording capability of the SUN interface.

reported to elicit natural touch perception,^[4–6] and intracortical microstimulation of the primary somatosensory cortex has also been shown to evoke tactile sensations in patients that cannot benefit from peripheral nerve sensory stimulation.^[7,8] These studies have started to use fairly dense electrode arrays (e.g., 2×4 mm electrode arrays with as many as 60 stimulation electrodes), which means that these arrays will not only be able to stimulate neurons that represent different parts of the body, but also neurons that represent different sensory modalities.^[9,10] Currently, artificial sensors are employed on the skin surface to collect sensory information for pressure,^[11–13] strain,^[14–16] and temperature.^[17–19] However, it is difficult for these artificial sensors to substitute the functions of the natural tactile and proprioceptive receptors due to their density and complexity. These peripheral receptors, together with the primary sensory neurons that relay their signals to the central

neural prostheses are assistive devices that restore lost functions resulting from neural damage.^[1] Sensory feedback plays an important role in improving the performance of the neural prostheses to achieve finer movement control.^[2,3] Electrical stimulation on the peripheral nerves in amputees has been

nervous system, are typically intact in persons with tetraplegia due to spinal cord injury. Recording of sensory signals from these primary sensory neurons that are part of the peripheral nervous system (PNS), and the transformation of the information into a feedback signal, provides an alternative^[20,21] but yet relatively unexplored way to restore high-fidelity sensory feedback to persons with tetraplegia. With the recent developments of implantable self-powered energy harvesters,^[22–24] it may now be possible to realize long-term nerve recording for sensory feedback.

The PNS of the upper and lower limb conveys both afferent sensory information to the brain and efferent motor commands to the muscles. Although the peripheral nerves are small in size, they are made up of several nerve fascicles holding hundreds of nerve fibers. As an example, the human median nerve trunk, which has around 20 nerve fascicles (with an average area of 0.16 mm^2), holds 20 000 axons.^[25] Thus, an effective neural interface needs to record from a large number of nerve fibers in a highly selective manner. To achieve this, various intrafascicular multichannel neural interfaces have been developed, including the longitudinal intrafascicular electrode (LIFE),^[26,27] the transverse intrafascicular multichannel

J. Wang, Dr. H. Wang, Dr. S. Lee, Prof. N. V. Thakor, Prof. S.-C. Yen, Prof. C. Lee

Department of Electrical and Computer Engineering
National University of Singapore

4 Engineering Drive 3, Singapore 117576, Singapore
E-mail: sinapsedirector@gmail.com; shihcheng@nus.edu.sg;
elec@nus.edu.sg

J. Wang, X. Y. Thow, Dr. S. Lee, Dr. K. Voges, Prof. N. V. Thakor,
Prof. S.-C. Yen, Prof. C. Lee

Singapore Institute for Neurotechnology (SINAPSE)
National University of Singapore
28 Medical Drive, #05-COR, Singapore 117456, Singapore

J. Wang, Dr. H. Wang, Dr. S. Lee, Prof. S.-C. Yen, Prof. C. Lee
Center for Intelligent Sensors and MEMS
National University of Singapore
4 Engineering Drive 3, Singapore 117576, Singapore

DOI: 10.1002/adhm.201700987

electrode (TIME),^[28,29] and the Utah Electrode Array (UEA).^[30,31] Different from LIFE and TIME, which are flexible interfaces threaded into the nerve, the UEA uses penetrating microneedles of customized height to access nerve fascicles. To extend the UEA along the nerve fiber direction, it is desirable to integrate the penetrating microneedle electrodes with a flexible substrate, which will deform with the nerve. A manually integrated stretchable microneedle electrode array has been shown to maintain stable contact with the muscle tissue during electromyographic recording and stimulation.^[32] However, the manual integration process lacks precision, repeatability, and scalability compared to standard microelectromechanical systems (MEMS) fabrication process. Thus, we hypothesize the combination of microneedles with flexible substrate using MEMS fabrication process will provide access to the nerve fascicles, while remaining flexible enough to accommodate small tissue movements.

Here, we report the development and application of a novel spiked ultraflexible neural (SUN) interface for recording from the PNS, which allows the subsequent decoding of sensory information. Polyimide was chosen here, due to the suitability of polyimide for long-term neural implants.^[33] It is a flexible, insulating material that can withstand tissue micromotion, and does not cause excessive inflammation. The novel structure enables the SUN interface to deform in accordance with nerve movements, while utilizing the penetrating spiked electrodes for intrafascicular recordings. In vivo experiments on the rat sciatic nerve demonstrated the capability of the SUN interface to detect small amplitude electroencephalogram (ENG) signals with a high signal-to-noise ratio (SNR). With these excellent recording capabilities of the SUN interface, we were able to differentiate tactile from proprioceptive stimuli. We further demonstrate that the signal was of the quality that a support vector machine (SVM) was able to classify the location of the stimulus with high spatial resolution.

Figure 1 shows the design and fabrication process of the SUN interface. The SUN interface features a polyimide substrate (with a Young's modulus of 2.5 GPa) with 20 μm thickness, rendering the device ultraflexible (Figure 1a). At one end of the device is a suture hole, which can be used to fix the device to the nerve epineurium. Distributed along the strip-like structure are: four spiked signal electrodes, one spiked reference electrode (all 300 μm in diameter), and one ground electrode (300 $\mu\text{m} \times 700 \mu\text{m}$). The strip-like structure serves as the main body of the SUN interface, as it sits on the nerve with its four signal electrodes penetrating the nerve, while both the reference and ground electrode remained outside the nerve close to the surrounding tissue. Underneath the top polyimide insulation layer, 50 μm width metal traces connect the electrodes to the connection pad located on the opposite end of the suture hole. This connection pad was specifically designed to fit onto a flexible printed circuit connector for data readout.

Multiple electrodes implanted along the nerve fibers enable longitudinal selectivity, while spikes of different height can be customized during fabrication to achieve transversal selectivity. To our knowledge, this unique combination of flexible substrate with rigid penetrating electrodes for nerve recording has never been reported previously. As shown in Figure 1b, the height of the spiked electrodes changes with the fabrication temperature. This control of the spike height allows targeting of different fascicles prior to implantation. Since the diameter of the sciatic nerve in a rat is ≈ 1 mm, 500 μm height spike structures were used to record from the center of the sciatic nerve.

The fabrication followed multilayer MEMS process (Figure 1c). To integrate the 3D spiked electrode structures on ultraflexible polyimide substrate, first, four-beam SU-8 pillars were fabricated with photolithography. These SU-8 pillars served as the base for double drawing lithography process to form sharp spiked electrode structures. Double drawing

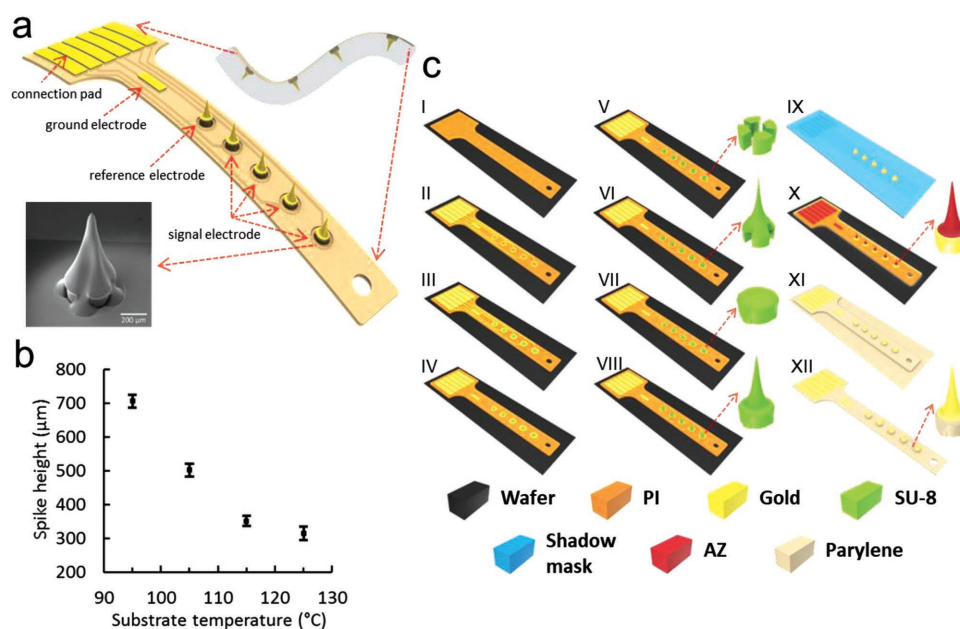


Figure 1. Design and fabrication of the SUN interface. a) Schematic of the SUN interface, with diagram of the SUN interface implanted on the sciatic nerve. b) Customization of SU-8 drawing lithography process to form the structures. Data presented as mean \pm s.e.m. ($n = 10$). c) Fabrication process.

lithography process was developed to improve the electrical connection between the 3D spiked electrode and bottom electrode. After the first drawing lithography process, the device was heated to allow the reflow of SU-8. This formed a gradual connection between the spike structure and the bottom electrode, resulting in a better electrical connectivity by later metal sputtering. Finally, the SUN interface was released from the wafer substrate, with all the area electrically insulated, except for the spike tips, ground electrode, and connection pads. The details of the fabrication process are provided in the Supporting Information.

In order to compare the *in vivo* ENG recording capabilities, an extraneural interface, and the intrafascicular SUN interface were implanted on the exposed left sciatic nerve of different rats (Figure 2a). The extraneural interface (Figure 2b) shares the same structural design with the SUN interface (Figure 2c), with the exception that the spike electrodes were replaced by planar electrodes with the same diameter. For both interfaces, the signal electrodes were numbered sequentially in accordance to their position: E4 was close to the suture hole, which in our experiment was implanted close to the sciatic nerve's trifurcation, where

it branched into three finer nerves; E1 was on the opposite end, close to the connector, and implanted proximal to the spinal cord.

The recording capability of both interfaces was assessed by measuring the impedance magnitude at 1 kHz prior to implantation in saline and 15 min after implantation. As shown in Figure 2d, the impedance magnitude in the SUN interface slightly increased upon implantation, but still remained within a desirable range of 10 k Ω to provide a good SNR.^[34] However, the impedance magnitude of the extraneural interface increased by several times. This large increase in impedance magnitude indicated that the electrode–tissue contact of the extraneural interface was not ideal, even though the interface was tightly wrapped around the nerve. This poor impedance magnitude might have resulted from microscale gaps between the electrode and tissue, as a result of the uneven bending of the extraneural electrode surface when trying to conform to the nerve. The electrically insulating epineurium surrounding the nerve might also have led to this impedance magnitude increase. In contrast, the spikes of the SUN interface were tightly surrounded by nerve fibers and consequently resulted in a much better electrode–tissue contact.

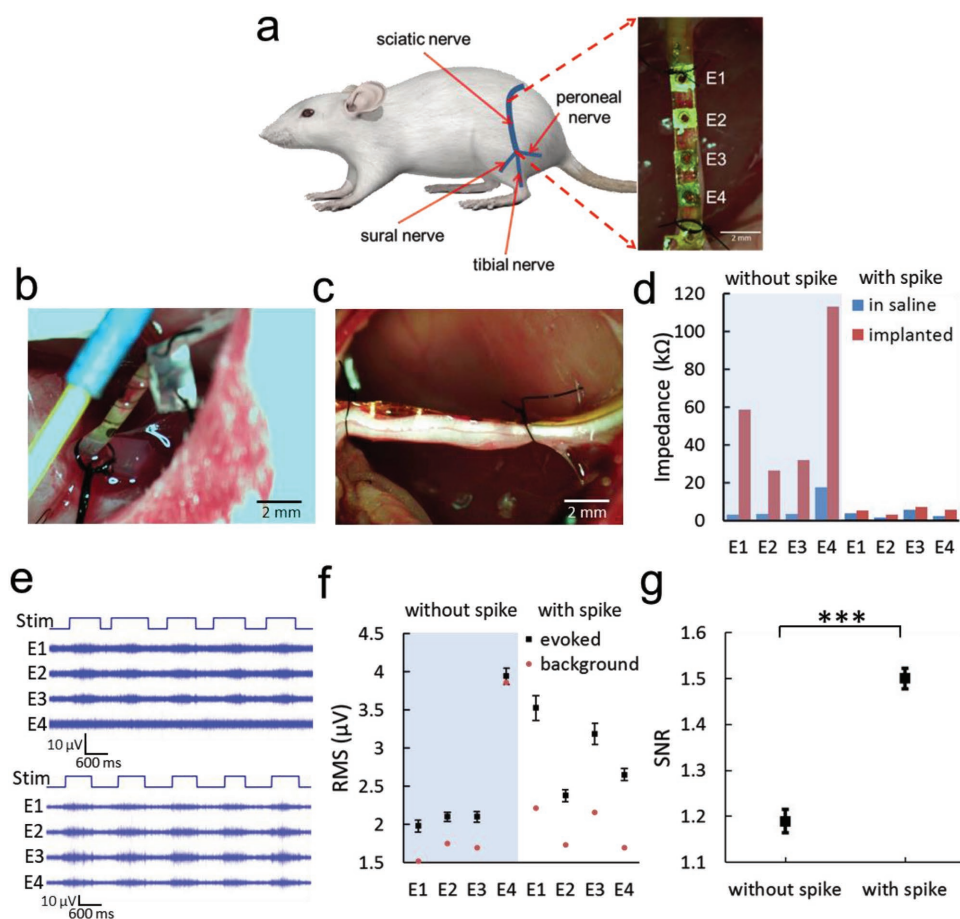


Figure 2. Comparison of ENG recording using an extraneural interface and the SUN interface. a) Positioning of the SUN interface on the rat's left sciatic nerve. Implantation of b) the extraneural interface, and c) the SUN interface. d) Impedances of both interfaces. e) ENG recordings in response to limb flexion. f) RMS comparison. g) SNR comparison. Data presented as mean \pm s.e.m. ($n = 20$). Statistical significance was indicated using *** for $p < 0.001$.

Next, proprioceptive sensory ENG was recorded with both electrodes (Figure 2e) and the SNR was compared. To induce proprioceptive sensory signals, the paw of the freely hanging left leg was gently pushed forward using a pair of forceps. The root mean square (RMS) was calculated for both baseline (no stimulus) and evoked recordings (Figure 2f), to quantitatively assess the difference in the ENG signals recorded with both electrodes. Subsequently, the SNR was calculated as the evoked RMS divided by the background RMS (Figure 2g). There was a significant difference between the SNR using the extraneural and the SUN interface (unpaired Student's *t*-test, $n = 20$, $p < 0.001$, t -value = 9.08), with the mean SNR increasing from 1.2 to 1.5.

Thus, the SUN interface, with the desired lower impedances after implantation, achieved ENG recordings with a sufficiently high SNR. The change in impedance measured prior to implantation (in saline) and after implantation can serve as an indicator of the quality of the electrode–tissue contact. This is because impedance measurement in saline simulates “perfect” electrode–tissue contact conditions, with conductive liquid perfectly surrounding the electrodes. Analogously, the SUN interface also achieved higher SNR during the in vivo ENG

recordings—the electrode tips were surrounded tightly by nerve tissues, and this resulted in direct contact with the nerve fibers.

Since the SUN interface achieved ENG recordings with higher SNR, in the ensuing experiments, we wanted to assess whether the recording capability of the SUN interface could provide peripheral nerve sensory information that could be satisfactorily decoded. Three subtle mechanical stimuli, either tactile or proprioceptive, were applied to the left paw of the animal: brushing (the paw was gently brushed with a pair of grounded metal forceps), pressing (the paw was lightly gripped with the forceps), and ankle flexing (the freely hanging left leg was gently pushed from the plantar paw surface to flex forward). The resulting band-pass filtered signals (with cutoff frequency of 0.4 and 2.2 kHz) are shown in Figure 3a. Power spectrum density (PSD) of the raw evoked ENG is shown in Figure 3b. With the PSD analysis of the spontaneous ENG and EMG (Figure S8, Supporting Information), we could confirm that the low frequencies distribution was induced by cyclical body movement artifacts and unwanted EMG signals detected by the nerve recording electrodes. Thus, a band-pass filter with cutoff frequencies of 0.4 and 2.2 kHz was chosen to remove the low frequency noise in our recordings. Spikes (i.e., compound nerve action potentials,

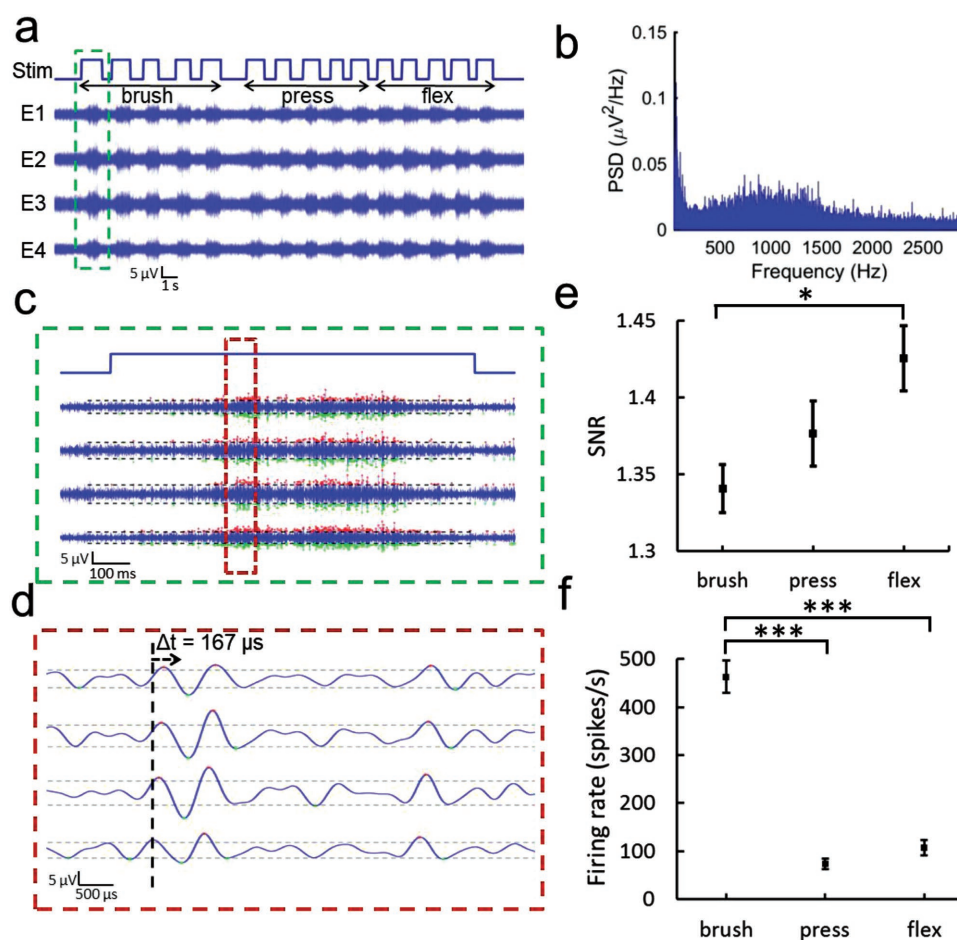


Figure 3. Discrimination of sensory modalities. a) ENG recording with the SUN interface. b) PSD of the raw evoked ENG recording. c) Spike detection results. d) Time delay of the spike peaks. e) SNR of three mechanical stimuli. f) Firing rate for each stimulus. Data presented as mean \pm s.e.m. ($n = 20$). Statistical significance was indicated using * for $p < 0.05$, and *** for $p < 0.001$.

CNAPs), were then detected using amplitude thresholds set for each channel (shown in dashed lines in Figure 3c).

Since action potentials from the stimulated sensory receptors transmitted through the sciatic nerve from the paw (distal) to the spinal cord (proximal), the ENG signals sequentially passed from E4 to E1 in our implantation configuration (Figure 3d). Therefore, peaks of the same detected spike showed a time-delayed pattern along the four channels: spikes from E4 appeared first, while spikes from E1 appeared last, with a time delay of 167 μs . Since the distance between E4 and E1 was 6 mm, we calculated the ENG transmission velocity to be 36 m s^{-1} , which was in agreement with the reported transmission velocity for $A\alpha$ nerve fibers in the rat.^[35]

In Figure 3e, the SNR extracted from the ENG evoked by the brushing stimulus was significantly different from that evoked by the flexing stimulus (one-way analysis of variance using Tukey's multiple comparisons test, $n = 20$, $p < 0.001$, $F = 4.79$). Here, the SNR value was comparable to the results reported by Navarro and co-workers^[20] and Micera and co-workers.^[21] Navarro and Micera noted that the rat sciatic nerve contained clusters of large myelinated fibers, similar to the $A\alpha$ and $A\beta$ fibers found in the human sciatic nerve.^[36] Earlier studies also found

smaller unmyelinated axons that could correspond to the $A\delta$ fibers.^[37] Thus, it is likely that the distribution of the different axon types is comparable across species.

In humans, tactile and pressure stimuli interact with surface mechanoreceptors, which have multiple subtypes corresponding to different firing rates^[38] and are transmitted by the $A\beta$ and $A\delta$ fibers.^[20] In contrast, proprioceptive information comes from the muscle spindles and is transmitted by the $A\alpha$ fibers.^[36] Thus, we wanted to know if the different firing rates exhibited by the different sources of sensory information could be discriminated in our experiments. We counted the spikes that occurred during the stimulation period, and divided them by the stimulus duration to obtain the firing rates (Figure. 3f). As expected, the firing rates elicited by the brushing stimulus was significantly different from those evoked by the pressing and flexing stimulus (one-way analysis of variance using Tukey's multiple comparisons test, $n = 20$, $p < 0.001$, $F = 97.98$). Firing rates between pressing and flexing stimuli were not significantly different. This might have been due to the application of insufficient pressure to fully activate the $A\delta$ fibers that encode pressure on the paw. These smaller fibers are expected to produce smaller amplitude compound action potentials, resulting in lower SNR.

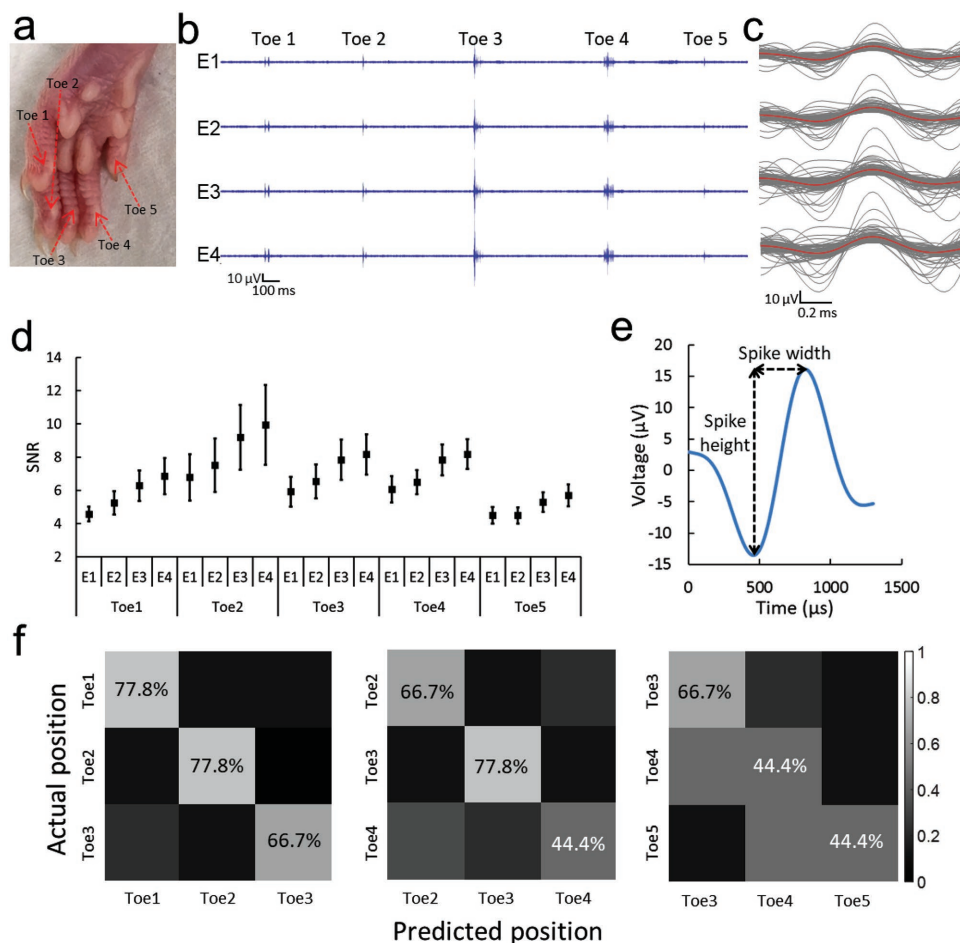


Figure 4. Discrimination of sensory stimulation location, a) Picture of the left toes in the animal. b) ENG recording in response to toe pinching. c) Superimposed ENG spike; individual spikes (gray) and averaged spike (red). d) SNR of toe pinching. e) Spike height and width definition. f) SVM classifier results, presented as mean \pm s.e.m. ($n = 20$).

Next, we conducted experiments to examine the capability of the SUN interface to differentiate stimulus locations on the rat's paw. We applied pinching stimuli to each toe in sequential order: from Toe1 to Toe5 (Figure 4a), and the band-pass filtered ENG recordings are shown in Figure 4b. Each toe was pinched with grounded metal forceps, without inducing any observable muscle movement. Spikes were detected using amplitude thresholds. Next, all the detected spikes (gray) were aligned using the peak of the spike, and superimposed on top of each other. The average spike waveform on each channel is shown in red (Figure 4c).

The SNR was calculated as before during each toe pinch (Figure 4d). Since toe pinching was more forceful than the other subtle mechanical stimuli used in the experiments, the recorded ENG had a much higher SNR. The CNAPs consisted of signals transmitted at different velocities by nerve fibers of different diameters, which led to temporal dispersion when the CNAPs were recorded over a larger distance. This temporal dispersion resulted in the separation of nerve signals transmitted by different nerve fibers, and the smaller CNAPs may not be detected by the amplitude threshold. Therefore, the SNR measured for the same toe but with different electrodes exhibited a descending pattern: it was the highest for E4 and the lowest for E1. Due to the similarity of the SNR measured for each toe, we were not able to differentiate the stimulus applied to different toes using the SNR.

Discrimination of the toe pinching location was next achieved with more detailed features extracted from the signals. Since the spike width and spike height are parameters generally used for examining the quality of ENG recordings,^[39] these two features were chosen to train a SVM classifier. With the extracted CNAP height and width features defined as in Figure 4e, all detected spikes were divided into three clusters with a *k*-means unsupervised classifier. Then, the count in each cluster was put into an SVM classifier. The SVM classifier was trained to discriminate between the responses evoked by pinching three of the toes at a time. The SVM classification results in Figure 4f show an average accuracy of 74.1% for discriminating between pinching stimuli on Toe1, Toe2, and Toe3, 63.0% for discriminating Toe2, Toe3, and Toe4, and 51.9% for discriminating Toe3, Toe4, and Toe5.

As shown in Figure 4f, the SVM classifiers achieved good discrimination among Toe1, Toe2, and Toe3. However, poor discrimination between Toe2 and Toe4, and between Toe4 and Toe5, diminished the overall performance of the three-toe classifiers. We trained another set of SVMs to examine the two-toe classifier performance for 1) Toe1 and Toe4; 2) Toe1 and Toe5; and 3) Toe2 and Toe5. The SVM classifiers showed good performance except for differentiating Toe1 and Toe4 (shown in Figure S8, Supporting Information). Thus, with exception of Toe4, the SVM classifiers achieved good performance for the two-toe discrimination. There are two reasons that can explain the limited performance of these SVM classifiers. First, the four signal electrodes might have recorded from the same nerve fascicles, as the spiked electrodes shared the same height and were implanted parallel to the nerve fascicle. Multiple spike electrodes of different heights would enable access to different nerve fascicles to collect sensory information for more accurate decoding. Second, the extraction of the CNAP height and width features

might have caused some information originally conveyed by the nerve signal to be lost. In order to decode more accurately, more electrodes accessing different nerve fibers, along with the use of other spike waveform features (e.g., shape) would likely enable better performance of the SVM classifiers.

In summary, we report a novel SUN interface that combines two highly desirable properties for nerve recording—flexible substrate to achieve conformal attachment to small nerves, and penetrating electrodes for high-quality intrafascicular nerve recording. Furthermore, we showed recording and subsequent decoding of sensory information from the PNS. With the intrafascicular SUN interface, we recorded small-amplitude ENG signals with high SNR, which were decoded to differentiate between different types of mechanical stimuli. By examining the firing rates of three different mechanical stimuli on the paw, we differentiated brushing from pressing and flexing actions. Furthermore, with four channel recordings, we achieved reasonably good performance using an SVM for spatial differentiation of sensory stimulation delivered to different toes.

Currently, sensory recording with the SUN interface is tested in acute animal experiments. Challenges still remain for future chronic implantations of the SUN interface to successfully record and decode sensory information from the PNS. One challenge is related to the potential foreign body reaction of the nerve tissue. The formation of extensive fibrotic scar tissue can effectively displace the implanted electrodes from the nerve tissue, which may result in sharp drops in the SNR, eventually leading to the complete loss of the neural signal.^[40,41] Another challenge involves the mixture of sensory signal with motor signal when the animal is moving around. In the acute experiments, the animal was under anesthesia, so the movement of the animal was eliminated. However, in chronic implantation, the recorded nerve signal is a mixture of sensory signal and motor signal, which will make the extraction and decoding of sensory information more challenging than in the acute animal test. Thus, further work remains to be done to assess the chronic recording capability of the SUN interface.

Experimental Section

Animal Surgery: Four Sprague–Dawley rats (around 250 g) were used for the sciatic nerve implantations. Anesthesia was induced with a mixture of Xylazine (7.5 mg kg⁻¹ IP) and Ketamine (50 mg kg⁻¹ IP) in 0.9% NaCl. Carprofen (5 mg mL⁻¹) was injected for pain relief before the surgery. After the rat was anesthetized, fur on the left leg was gently removed by a shaver. Then, the skin was disinfected with 70% ethanol wipes, and an incision was made with a surgical blade to expose the bicep femoris muscle. After separating the bicep femoris muscle into two halves, the sciatic nerve was visible. To separate the sciatic nerve from nearby muscles, the fat tissue surrounding the sciatic nerve was carefully removed with sharp-tip tweezers under a microscope. The extraneural interface was wrapped around the sciatic nerve, with all the electrodes facing the nerve tissue. Since close contact between the electrode interface and the tissue was crucial to record small-amplitude ENG signal for the extraneural interface, the device was wrapped tightly around the nerve with no observable nerve compression under the microscope. When it came to the SUN interface, the spikes were implanted in the nerve sequentially. For each of the spikes, a suture needle was used to slightly break the epineurium around the projected penetration site. Then, with a sharp-tip tweezer pushing from the backside of the SUN interface,

the spike was inserted into the nerve. Throughout the surgery, anesthesia was topped up every hour and the heart rate and body temperature of the animal was carefully monitored. After the nerve recording was completed, a 2% Lignocaine gel (Lidocaine) was applied to the nerve to create a temporary nerve block. All the procedures were performed under protocol 143/12 and approved by the Institutional Animal Care and Use Committee at the National University of Singapore.

Neural Recording and Signal Processing: All ENG recordings were amplified with the RHD2132 evaluation system (Intan Technologies). The sampling rate was 30 kHz. Impedance measurements in saline and after implantation were performed with the same system at 1 kHz. The current generator of the Intan chip applies a small-amplitude AC current on the signal and reference electrodes, and the voltage is recorded by the Intan chip. Impedance was measured as the ratio of peak voltage to peak current. Data processing was performed using MATLAB software (MathWorks). After examining the PSD of the ENG recordings, a band-pass filter with cutoff frequencies of 0.4 and 2.2 kHz was applied to remove the low frequency noise induced by movement artifact,^[42] and electromyography (EMG).^[43,44]

Identifying Pressure Stimulation Periods: The analog pressure signal recorded using a pressure sensor attached to a pair of forceps was digitized using the RHD2132 evaluation system (Intan Technologies) at a sampling rate of 30 kHz. Next, the mean and standard deviation of the background (i.e., when no pressure was applied) signal were calculated. A threshold was set to the mean plus three times the standard deviation. The start of the pressure stimulus was identified when ten consecutive points exceeded the threshold, and the end of the stimulus was when ten consecutive sampling points fell below the threshold. In the figures, the pressure stimulation periods are depicted to have a value of 1, while the remaining periods are depicted to have a value of 0.

Threshold for Spike Detection: Spikes were detected on amplitude basis. First, the mean and standard deviation of the background ENG recording were calculated. The first 1000 ENG points before the start of stimulation were used as the background signal. Then, an upper (or lower) threshold was established as mean plus (or minus) three times the standard deviation. A spike was identified when five consecutive ENG points exceeded the threshold, and was marked as red (or green) on the peak (or valley) in Figure 3b.

SVM Classifier for Discriminating Toe Stimuli: First, spikes were detected on amplitude basis for nine trials of recording. Then spike height and spike width feature, as defined by Nowotny et al.,^[39] were extracted for all spikes recorded by four channels. These two features formed a 2D description of all detected spikes. Then, a *k*-means unsupervised classifier was used to divide the spikes into three clusters. These three clusters were characterized as: large spike height, small spike width; small spike height, small spike width; and small spike height, large spike width. For each toe stimulus, the spike number in each cluster was counted for each of the four channels and summed together. Thus, each toe stimulus was characterized by three spike counts in the three clusters. Quadratic SVM classifiers with fivefold cross validation were then used to learn and quantify the differences between the signals when a stimulus was applied to each of the three toes.

Statistical Analysis: Statistical comparisons were performed using MATLAB. All data were presented as mean \pm s.e.m. (with $n = 20$ samples) unless otherwise stated. For the comparison between the SNR extracted from the ENG recorded with the extraneural interface and the SUN interface, the unpaired Student's *t*-test was used. For comparing the firing rates of brushing, pressing and flexing stimuli, one-way analysis of variance using Tukey's multiple comparisons test was performed, with the *p*-value adjusted to account for multiple comparisons. Statistical significance was indicated using * for $p < 0.05$, and *** for $p < 0.001$.

Supporting Information

Supporting Information is available from the Wiley Online Library or from the author.

Acknowledgements

This work was supported by the following grant from the National Research Foundation: Competitive Research Project 'Peripheral Nerve Prosthesis: A Paradigm Shift in Restoring Dexterous Limb Function' (NRF-CRP10-2012-01).

Conflict of Interest

The authors declare no conflict of interest.

Keywords

biomaterials, flexible electronics, neural interfaces, peripheral nervous system, sensory decoding

Received: August 18, 2017

Revised: September 4, 2017

Published online: December 4, 2017

- [1] A. Prochazka, V. K. Mushahwar, D. B. McCreery, *J. Physiol.* **2001**, 533, 99.
- [2] G. S. Dhillon, K. W. Horch, *IEEE Trans. Neural Syst. Rehabil. Eng.* **2005**, 13, 468.
- [3] I. Saunders, S. Vijayakumar, *J. Neuroeng. Rehabil.* **2011**, 8, 60.
- [4] S. Raspopovic, M. Capogrosso, F. M. Petrini, M. Bonizzato, J. Rigos, G. Di Pino, J. Carpaneto, M. Controzzi, T. Boretius, E. Fernandez, *Sci. Transl. Med.* **2014**, 6, 222ra19.
- [5] D. W. Tan, M. A. Schiefer, M. W. Keith, J. R. Anderson, J. Tyler, D. J. Tyler, *Sci. Transl. Med.* **2014**, 6, 257ra138.
- [6] T. Davis, H. Wark, D. Hutchinson, D. Warren, K. O'Neill, T. Scheinblum, G. A. Clark, R. Normann, B. Greger, *J. Neural Eng.* **2016**, 13, 036001.
- [7] S. N. Flesher, J. L. Collinger, S. T. Folds, J. M. Weiss, J. E. Downey, E. C. Tyler-Kabara, S. J. Bensmaia, A. B. Schwartz, M. L. Boninger, R. A. Gaunt, *Sci. Transl. Med.* **2016**, 8, 361ra141.
- [8] L. Johnson, J. Wander, D. Sarma, D. Su, E. Fetz, J. G. Ojemann, *J. Neural Eng.* **2013**, 10, 036021.
- [9] R. M. Friedman, L. M. Chen, A. W. Roe, *Proc. Natl. Acad. Sci. USA* **2004**, 101, 12724.
- [10] T. Tomlinson, L. E. Miller, in *Progress in Motor Control*, Springer, **2016**, 367.
- [11] B. C.-K. Tee, A. Chortos, A. Berndt, A. K. Nguyen, A. Tom, A. McGuire, Z. C. Lin, K. Tien, W.-G. Bae, H. Wang, *Science* **2015**, 350, 313.
- [12] L. Pan, A. Chortos, G. Yu, Y. Wang, S. Isaacson, R. Allen, Y. Shi, R. Dauskardt, Z. Bao, *Nat. Commun.* **2014**, 5.
- [13] B. C. K. Tee, A. Chortos, R. R. Dunn, G. Schwartz, E. Eason, Z. Bao, *Adv. Funct. Mater.* **2014**, 24, 5427.
- [14] T. Yamada, Y. Hayamizu, Y. Yamamoto, Y. Yomogida, A. Izadi-Najafabadi, D. N. Futaba, K. Hata, *Nat. Nanotechnol.* **2011**, 6, 296.
- [15] F. Cellini, S. Khapli, S. Peterson, M. Porfiri, *Appl. Phys. Lett.* **2014**, 105, 061907.
- [16] D. J. Lipomi, M. Vosgueritchian, B. C. Tee, S. L. Hellstrom, J. A. Lee, C. H. Fox, Z. Bao, *Nat. Nanotechnol.* **2011**, 6, 788.
- [17] N. T. Tien, S. Jeon, D. I. Kim, T. Q. Trung, M. Jang, B. U. Hwang, K. E. Byun, J. Bae, E. Lee, J. B. H. Tok, *Adv. Mater.* **2014**, 26, 796.
- [18] T. Yokota, Y. Inoue, Y. Terakawa, J. Reeder, M. Kaltenbrunner, T. Ware, K. Yang, K. Mabuchi, T. Murakawa, M. Sekino, *Proc. Natl. Acad. Sci. USA* **2015**, 112, 14533.

- [19] R. C. Webb, A. P. Bonifas, A. Behnaz, Y. Zhang, K. J. Yu, H. Cheng, M. Shi, Z. Bian, Z. Liu, Y.-S. Kim, *Nat. Mater.* **2013**, 12, 938.
- [20] J. Badia, S. Raspopovic, J. Carpaneto, S. Micera, X. Navarro, *IEEE Trans. Neural Syst. Rehabil. Eng.* **2016**, 24, 20.
- [21] S. Raspopovic, J. Carpaneto, E. Udina, X. Navarro, S. Micera, *J. Neuroeng. Rehabil.* **2010**, 7, 17.
- [22] Q. Zheng, Y. Zou, Y. Zhang, Z. Liu, B. Shi, X. Wang, Y. Jin, H. Ouyang, Z. Li, Z. L. Wang, *Sci. Adv.* **2016**, 2, e1501478.
- [23] Q. Zheng, B. Shi, F. Fan, X. Wang, L. Yan, W. Yuan, S. Wang, H. Liu, Z. Li, Z. L. Wang, *Adv. Mater.* **2014**, 26, 5851.
- [24] Z. Li, G. Zhu, R. Yang, A. C. Wang, Z. L. Wang, *Adv. Mater.* **2010**, 22, 2534.
- [25] I. Delgado-Martínez, J. Badia, A. Pascual-Font, A. Rodríguez-Baeza, X. Navarro, *Front. Neurosci.* **2016**, 10.
- [26] S. M. Lawrence, G. Dhillon, W. Jensen, K. Yoshida, K. W. Horch, *IEEE Trans. Neural Syst. Rehabil. Eng.* **2004**, 12, 345.
- [27] S. M. Lawrence, G. S. Dhillon, K. W. Horch, *J. Neurosci. Methods* **2003**, 131, 9.
- [28] T. Boretius, J. Badia, A. Pascual-Font, M. Schuettler, X. Navarro, K. Yoshida, T. Stieglitz, *Biosens. Bioelectron.* **2010**, 26, 62.
- [29] J. Badia, T. Boretius, A. Pascual-Font, E. Udina, T. Stieglitz, X. Navarro, *IEEE Trans. Biomed. Eng.* **2011**, 58, 2324.
- [30] A. Branner, R. B. Stein, E. Fernandez, Y. Aoyagi, R. A. Normann, *IEEE Trans. Biomed. Eng.* **2004**, 51, 146.
- [31] A. Branner, R. B. Stein, R. A. Normann, *J. Neurophysiol.* **2001**, 85, 1585.
- [32] G. S. Guvanasesan, L. Guo, R. J. Aguilar, A. L. Cheek, C. S. Shafor, S. Rajaraman, T. R. Nichols, S. P. DeWeerth, *IEEE Trans. Neural Syst. Rehabil. Eng.* **2016**.
- [33] P. J. Rousche, D. S. Pellinen, D. P. Pivin, J. C. Williams, R. J. Vetter, D. R. Kipke, *IEEE Trans. Biomed. Eng.* **2001**, 48, 361.
- [34] S. Lee, S. Sheshadri, Z. Xiang, I. Delgado-Martínez, N. Xue, T. Sun, N. V. Thakor, S.-C. Yen, C. Lee, *Sens. Actuators, B* **2017**, 242, 1165.
- [35] A. Harper, S. Lawson, *J. Physiol.* **1985**, 359, 47.
- [36] V. G. Macefield, *Clin. Exp. Pharmacol. Physiol.* **2005**, 32, 135.
- [37] H. Schmalbruch, *Anat. Rec.* **1986**, 215, 71.
- [38] K. O. Johnson, *Curr. Opin. Neurobiol.* **2001**, 11, 455.
- [39] T. Nowotny, J.-P. Rospars, D. Martínez, S. Elbanna, S. Anton, *PLoS One* **2013**, 8, e80838.
- [40] G. C. McConnell, H. D. Rees, A. I. Levey, C.-A. Gutekunst, R. E. Gross, R. V. Bellamkonda, *J. Neural Eng.* **2009**, 6, 056003.
- [41] R. Biran, D. C. Martin, P. A. Tresco, *J. Biomed. Mater. Res., Part A* **2007**, 82, 169.
- [42] C. J. De Luca, L. D. Gilmore, M. Kuznetsov, S. H. Roy, *J. Biomech.* **2010**, 43, 1573.
- [43] P. Grosse, M. Cassidy, P. Brown, *Clin. Neurophysiol.* **2002**, 113, 1523.
- [44] B. Bigland-Ritchie, E. Donovan, C. Roussos, *J. Appl. Physiol.* **1981**, 51, 1300.